# Journal of Materials Chemistry C

Accepted Manuscript

This article can be cited before page numbers have been issued, to do this please use: D. S. Saranin, V. Mazov, L. O. Luchnikov, D. Lypenko, P. A. Gostishev, D. Muratov, D. A. Podgorny, . M. Migunov, S. I. Didenko, M. Orlova, D. Kuznetsov, A. R. Tameev and A. Di Carlo, *J. Mater. Chem. C*, 2018, DOI: 10.1039/C8TC01169A.




ROYAL SOCIETY OF CHEMISTRY

rsc.li/materials-c

View Article Online
DOI: 10.1039/C8TC01169A

View Article Online
DOI: 10.1039/C8TC01169A

Journal Name

ARTICLE

# Tris (ethylene diamine) nickel acetate as a promising precursor for hole transport layer in planar structured perovskite solar cells

Received 00th January 20xx,
Accepted 00th January 20xx

DOI: 10.1039/x0xx00000x

www.rsc.org/

Danila S. Saranin*[a], Vsevolod N. Mazov[a], Lev O. Luchnikov[a], Dmitry Lypenko[b], Pavel A. Gostishev[a], Dmitry S.Muratov[a], Dmitry A. Podgorny[c], Denis M. Migunov[d], Sergei I. Didenko[a,e], Marina N. Orlova[e], Denis V. Kuznetsov[a,f], Alexey R. Tameev[b] and Aldo Di Carlo*[a,g]

Owing hysteresis free characteristics and good reproducibility, inverted p-i-n Perovskite Solar Cells (PSC) are gaining large interest in the photovoltaic field. In this contest, the request for stable materials calls for the development of robust transporting layers compatible with the fabrication processes of the solar cell. In this paper we introduce a new precursor, the tris (ethylene diamine) nickel acetate, for low temperature (280-300 °C) deposition of NiO hole transporting layer. A full characterization of the deposited NiO film layer is performed by using a combined investigation comprising XRD, Raman and Auger spectroscopy. We found a direct correlation between device performance and NiO thickness with maximum efficiency, exceeding 15%, reached for the thinner NiO (10nm) layer.

## Introduction

The unprecedented progress in the development of organic-inorganic hybrid perovskite solar cells (PSC) have attracted the attention of the scientific community even beyond the photovoltaics (PVs) field. The rapid growth of power conversion efficiency (PCE) from 3.8% of the 2009 pioneer work[1] to the current certified record PCE of 22.7%[2] show the PSC technology on par with more traditional Si, CiGS and CdTe solar cells[3–5]. The highest device performances have been achieved in mesoscopic n-i-p architecture[6], where light is imping on the n side of the cell, that is from the Electron Transporting Layer (ETL) side, and a mesoscopic scaffold is used to grow the perovskite absorber layer. ETLs, typically based on $TiO_2$, suffer from interface degradation and instability caused by the absorption of ultraviolet part of the light[7–9]. UV absorption tends to increase the concentration of trap states and parasitic charge accumulation that contributes to hysteresis effects[10–12] and to the overall stability of the cell[13]. Moreover, hole transport materials (HTMs) used for highly efficient PSCs[14], such as SPIRO–OMeTAD require Li and/or Co based salts doping to increase hole conductivity[15,16] which, in turn, can compromise the cell stability leading to PSC degradation[17,18], extrinsic ion migration[19] and charge trapping near the HTM[20] .

One of the strategies to avoid the limits of the n-i-p configuration described above consists in the inverted (p-i-n) PSC architecture[21]. Here the light is impinging from the HTM side which can be realized with polyelectrolytes (PEDOT:PSS and etc.)[22], polymers (PTAA and etc.)[23] and inorganic materials[24]. As discussed in several works[25,26] p-i-n devices with inorganic HTMs have better interface stability and lower material costs in comparison to n-i-p structures. A number of inorganic HTMs such as copper thiocyanate (CuSCN)[27,28], copper iodide (CuI)[29], and metal oxides ($V_2O_5$[30], CuO[31,32] $MoO_x$[33] and NiO[34,35]), show very promising device performance.

[a] L.A.S.E. - Laboratory for Advanced Solar Energy, National University of Science and Technology "MISiS" 119049 Leninskiy prospect ,. Moscow, Russia
[b] Laboratory "Electronic and photon processes in polymer nanomaterials", Russian academy of sciences A.N. Frumkin Institute of Physical chemistry and Electrochemistry, 119071 Leninskiy prospect 31k4. Moscow, Russia
[c] Department of Material Science in Semiconductors and Dielectrics, National University of Science and Technology "MISiS", 119049 Krymskiy val 3. Moscow, Russia
[d] R&D center "Microsystem technique and the bases of electronic components", National Research University of Electronic Technology, 124527, Solnechnaya alley 6, Zelenograd, Moscow, Russia
[e] Department of Semiconductor Electronics and Device Physics, National University of Science and Technology "MISiS" 119049 Krymskiy val 3, Moscow, Russia
[f] Department of Functional NanoSystems and High- Temperature Materials, National University of Science and Technology "MISiS" 119049 Leninskiy prospect 4, Moscow, Russia
[g] CHOSE - Centre for Hybrid and Organic Solar Energy, Department of Electronic Engineering, University of Rome Tor Vergata, 00133 via del Politecnico 1, Rome, Italy

*Corresponding authors:
Danila Saranin e-mail: danilasaranin@gmail.com
Professor Aldo Di Carlo e-mail: aldo.dicarlo@uniroma2.it
Electronic Supplementary Information (ESI) available: [details of any supplementary information available should be included here]. See DOI: 10.1039/x0xx00000x

DOI: 10.1039/C8TC01169A




In this work we focus on NiO considered a thermally stable hole transport layer (HTL) for p-i-n devices that induces negligible hysteresis[36] and, consequently, a maximum power output which is not penalized by this phenomenon.[37] Moreover, as it was shown by *Corani et al.* [38], NiO provide ultrafast hole injection dynamics at the interface with $MAPbI_3$ due to a good energy level alignment.

Concerning PSCs with NiO HTL, *Yanagida et al.*[39] performed calculations of the carrier flux in NiO from Einstein-Smoluchowski relation and determined that NiO is able to compensate the photo-generated current density in perovskite layers up to a maximum theoretical value of 26 mA/cm$^2$. This limit has not yet been achieved in fabricated PSC with NiO showing the importance of further optimizations of this inorganic HTL by improving material purity and crystallinity. Vacuum processing such as magnetron sputtering and ALD can give excellent material purity, but it will raise up the production costs making, at the same time, the manufacturing integration more complex. Recently, NiO HTL with Cu[40], Li[41], Cs[42] doping have been considered to improve charge transport and collection in inverted PSCs reaching of top level PCE of 19%. For most of the cases, incorporation of metal dopants increases local conductivity, enhances photoluminescence quenching and raise hole mobility.

Solution-process formation of NiO on the top of the Transparent Conductive Oxide (TCO) requires a proper precursor solution and a subsequent thermal treatment to achieve optimal morphology of the films. One of the common ways to obtain NiO film is the decomposition of its complex compounds[43–47]. Changing the composition of the complex salt by the anion or ligands can significantly influence the decomposition temperature which is typically in the range of 300-750 °C[48–56]. A low temperature (LT) process, is highly desirable to permit the use of polymeric substrates for flexible PSCs[57]. Moreover, a high decomposition temperature will negatively impact on the price of the solar panel which is determined not only by the cost of materials used for its fabrication, but also by the amount of the energy used at each stage of the production process. Thus, in addition to switching to cheaper materials, it is necessary to reduce energy consumption at each step of the manufacturing process in order to decrease the energy payback time[58].

Conventionally, to decrease the formation temperature of a nickel oxide compact layer, ligands such as ethylene diamine, pyridine, and other low molecular weight nitrogen-containing organic substances are used[59,60]. A solution processed Cs-doped NiO HTL, with a precursor decomposition temperature of 275 °C, was shown by *Djurisic et al*[42]. They used ethanolamine as a complex builder for the NiO precursor and achieved a PCE >19%. *You et al*[61] presented improved air stability (PCE ~16 % during 60 days) inverted PSC with undoped NiO HTL obtained by decomposing at 300 °C nickel nitrate with ethylene diamine. Approximately the same level of performance was presented by *Groeneveld et al.*[62] with a nickel formate dihydrate precursor for the HTL fabrication. A different process with a higher decomposition temperature (350 °C) was shown by *Yin*[63] using of pure nickel nitrate hexahydrate. Other LT NiO deposition approaches were proposed by using self-assembling nanoparticles[64] or vacuum processing[65]. We should point out, however, that thermal decomposition of NiO with a process temperature as low as 200 °C has been reported by *Nazli Dınçer Kaya et al*[66]. However, the azide derivatives used in the process are extremely explosive and their decomposition leaves little traces of nickel oxide, thus a direct application to PSCs is not favorable. Thus, the search for novel precursors of NiO providing an LT deposition of this HTL is an active area of research and development for low temperature p-i-n perovskites. We should point out that the interface between NiO and perovskite is also ruling the final performance of the solar cell through interface trap density, energy level alignment, grain size, passivation and materials purity[67–69]. For this reason, a detailed assessment of the interface quality is required when discussing NiO based PSC.

In this work, we introduce a new precursor route for the formation of NiO HTL based on commercially available nickel acetate complex with ethylene diamine. This precursor permits a decomposition temperature around 280-300 °C still maintain a good cell performance and without the use of dopants. To support our new deposition strategy, we performed a complete characterization of nickel oxide film including precursor decomposition parameters, reaction yield and Raman spectroscopy. Moreover, depth-profiling analyses using Auger spectroscopy data confirms the phase, elemental composition of the layers and the well defines interfaces between Perovskite/NiO and NiO/FTO. Device output performance shows promising PCE >15 % and negligible hysteresis.

## Results and discussion

The new NiO precursor (image S1 in supplementary info (S.I.)), the tris(ethylenediamine) nickel acetate (TED-NiA), was obtained by a two step method as depicted in Fig. 1(a) and described in the experimental. Fourier transform infrared spectroscopy (FTIR) shown in Fig. 1(b) confirms the synthesis of the precursor with the typical peaks related to the amine groups (3400-3000 cm$^{-1}$), C=O- (1730 cm$^{-1}$) and CH2- (2840-2865 cm$^{-1}$ and 2916-2936 cm$^{-1}$). Due to the facile synthesis of the precursor crystals obtained from the evaporation of the reaction mixture, compounds with water in the coordination sphere could be present. This is confirmed by a thermogravimetric (TGA) study of TED-NiA presented in Fig 1(c). Individual steps of the process were determined by fitting the weight loss derivative with respect to temperature (derivative weight curve) with Gaussians. The first 3 peaks (65 °C, 157 °C and 195 °C) are related to moisture desorption, crystalline water and water evaporation from the coordination sphere of Ni, respectively. The fourth and the fifth peaks (at 215 °C and 252 °C) of the derivative weight are related to the decomposition of dehydrated TED-NiA into compact nickel oxide film. This process involves the formation of solid nickel oxide, with the production of CO, $CO_2$, $H_2O$ and $N_2$ gases. We

View Article Online
DOI: 10.1039/C8TC01169A






can consider nickel oxide reduction reaction due to the presence of CO which is related to the acetate salt decomposition[70]. Moreover, this process is clearly shown by the presence of two endothermal peaks on the heat flow curve at 215 °C and 252 °C. It should also be noted that some carbon could dissolve in nickel metal after the reduction process leading to the formation of solid solution or nickel carbides[71]. Nonetheless, TGA curve shows that the maximum weight loss rate is reached at 250 °C and full TED-NiA decomposition into nickel oxide is already completed at 280 °C.

The formation of NiO layer is also confirmed by the Raman spectrum reported in Figure 2(a), where the peaks are mainly related to NiO[72]. To further investigate the chemical composition of the produced nickel oxide compact layer and to identify additional compounds formed after the decomposition of the TED-NiA, we performed Auger electron spectroscopy measurements shown in Figure 2 (b). Auger data reveal the presence, beside of nickel and oxygen, of a comparable amount of carbon, and a negligible percentage of chlorine, which remains from the initial nickel chloride. The presence of carbon could be related to the dissolved carbon in nickel metal phase. Moreover, carbon and hydrocarbons can be adsorbed during the formation of the layer from the ambient atmosphere, and remain after decomposition process of TED-NiA complex. The presence of nitrogen was not detected, which is clear a signature of the decay of the coordination sphere. Investigation of the distribution of the basic elements by Auger depth profiling (Figure 2(c)) shows that nickel penetrates into the substrate and presents a partially pure metal form. The concentration of carbon in the NiO layer is significant and grows toward the surface of the oxide layer up to 70 at %. In order to determine surface quality we provided high-resolution (HR) scanning electron microscopy (SEM) imaging presented on fig 2d together with a 3D AFM reconstruction (fig.S2). HR SEM was done for NiO films on polished silicon substrates while the 3D reconstruction on FTO glass. We obtained a continuous film with surface uniformity in the scale of tens nanometers, confirming that NiO film is closely following the morphology of the substrate surface.

The thickness of this NiO layer was varied from 27 nm down to 10 nm by changing the concentration of the TED-NiA precursor from 2.0 M to 1.0 M, respectively. The relation between precursor concentration and the final film thickness is reported in Fig. 3(a). Further decreasing of TED-NiA concentration did not provide an enough compact HTL film to permit the fabrication of the PSC stack without microscopic pinholes.

XRD pattern of the 27nm thick NiO compact layer on Si wafer (fig.S3) shows the presence in the film of pure nickel, which is a product of nickel oxide reduction by CO gas produced on TED-NiA decomposition stage. Along with it, the pattern has low intensity nickel oxide bands, which could be explained by the fact that the coherent scattering region of NiSO nanocrystals is most likely less than 5 nanometers, close to the detection limit of the method. Pure nickel and nickel oxide XRD peaks determination confirmed with data from previous studies of this material[73,74]. Moreover, as demonstrated by the Auger profile (fig. 2c) the metallic Ni is placed at the interface between NiO and Silicon. We conclude that nickel oxide film is passivating pure nickel phase and stabilizing the compact layer.

In order to assess the hole extraction properties of NiO, we measured photoluminescence (PL) spectra on the glass/FTO/NiO/MAPI stack for different thicknesses of NiO layer. As shown in Fig. 3(b), the presence on NiO induce a clear quenching of the PL with respect to pure MAPI film indicating a reduction in radiative recombination of generated electron-holes and an enhanced hole extraction when NiO HTL is used. Moreover, PL quenching is higher for a NiO thickness of 10 nm while it reduces for higher thicknesses. As already reported for GO HTL [75] and ZnO ETL[76] the higher quenching of the PL for the thinnest NiO layer is related to the reduction of the NiO resistance by decreasing the thickness of the HTL. To prove this
we performed conductance measurements by varying the NiO thickness. Diode structures were fabricated on FTO substrates with the gold cathode and NiO film sandwiched in between. The relation between JV characteristics and NiO thickness is presented in figure S4(S.I.). Despite Shottky diode type structure used for testing, JV curves showed a resistor behavior without rectification due to the small thicknesses of semiconductor (~tens of nm) that permits the formation of an ohmic contact between NiO and FTO as also found for the same thin film diode structure[77]. As expected, a clear increase of resistance (reduction of the JV curve slope) is found by increasing the NiO thickness. Resistivity values extracted from diode JV curves (calculated with eq.S1 and presented in table S1) are in the range between 182-340 kOhm*cm and compare well with the results reported by *Jlassi et al.*[78] for solution processed NiO. These values of the NiO resistivity also can be related to the presence of impurities. As we can see from Auger data of Figs. 2(a),(b) beside NiO, HTL also contains nickel chlorine, carbides and probably carbonates, which were not removed completely during decomposition of TED-NiA. Such impurities can harm charge transport, create trap states and warp crystal structure. Similar effects of side impurities containment ($Ni(OH)_2$, $Ni_2O_3$ ) has been reported by *Icli et al*[79]. Moreover, we found a reduction of resistivity by decreasing the NiO thickness (fig. 3(a)). This could be related to the increase of majority charge density by reducing the NiO thickness as reported by *Thimsen et al*[77].

An additional feature of the PL spectra is related to the peak position which blue shifts from 782 nm in the glass/Perovskite to 772 nm in the glass/NiO (10nm)/Perovskite. PL Peak shift has been observed several time for NiO HTL in PSC[61,80], but only a few explanations have been provided. This effect has been mainly related to the passivation of trap states [81–83], however the presence of pure nanosized nickel in HTL (defined previously by XRD and Auger) can induce the appearance of plasmon effect which is typical for metal nanoparticles[84]. Nickel nanoparticles[85,86] absorb light

DOI: 10.1039/C8TC01169A




in the visible region and therefore can shift PL peak like it was presented by of *Liu et. al*[87] for Ag. This suggestion should be proved and confirmed with an additional investigation that is beyond the scope of the present work. In any case, the MAPI/NiO/FTO interface is well defined and sharp as demonstrated by the Auger depth profile recorded for the glass/FTO/NiO/MAPI stack (See Fig. S6).

Devices were fabricated in inverted planar configuration considering the FTO/NiO/CH3NH3PbI3/C60/ Bathocuproine (BCP)/Al stack sequence, as presented in Fig.4(a) together with the schematic band diagram (fig.5(b)) and cross section (fig.5(c)). The NiO HTL was deposited following the developed decomposition process described in the previous section. The measured photovoltaics parameters are reported in Fig. 5(a-d) and table S2 for several NiO thicknesses. The average PCE of the fabricated cells increases from ~10 % with a 28 nm NiO film to ~14.82 % when the film thickness is reduced down to 10 nm.

The JV characteristics of the most efficient cell are reported in Fig. 6 showing a PCE of 15.31 %. We observe a strong correlation between HTL thickness and short-circuit current (Jsc) and fill-factor (FF) values. With a NiO thickness of 27 nm the PSCs show poor performances with an average Jsc = 17.76 mA/cm2 and an average FF=0.51. By increasing the NiO thickness to 16nm, PSC characteristics where improved achieving and average Jsc of 18.38 mA/cm$^2$ (+ 3.5% with respect to PSCs with NiO thickness of 27 nm) and an average FF of 0.57 (+11.8%). The best results were obtained with the thinnest layer of NiO (10nm) with an average Jsc= 19.68 mA/cm$^2$ (+10.8%), and a large increase of average FF up to 0.74 (+45%). These improvements occurred with significant series resistance (Rs) reduction (presented in table S2 in supplementary) that corresponds to higher ohmicity of NiO-FTO junction for thinner NiO HTL as already presented in Fig.4. Open circuit voltage (Voc) shows a behaviour similar to other J-V parameters with the best values achieved for 1.0 M TED-NiA concentration, even though the increase of Voc by reducing the thickness of NiO from 27 nm to 10 nm is only 4%. The spread of PV parameters are mainly related to local uneven film thickness caused by FTO surface roughness (typically ~50 nm for used TEC-8), which is not levelled by thin NiO film. JV characteristics presented in Fig. 6 shows negligible hysteresis with a hysteresis index < 0.02 (calculated from equation S2). Also by varying the scan rates (22 mV/s, 135 mW/s, 345 mV/s) the hysteresis remain negligible as shown in supplementary figures S5(a-c). Attempts to decreasing the NiO thickness below 10nm by further diluting the TED-NiA concentration resulted in a reduced PSC performance due to a significant decrease of shunt resistance (FF < 0.35) caused by pinholes in the NiO film. Shelf life stability measurements (presented in Fig.S7) were performed in glovebox during 12 days. While $V_{oc}$ and $J_{sc}$ values were stable, FF lost ~ 30 % of the initial value and, consequently, affected the PCE. Stabilization of the device requires specific optimizations in the perovskite[88,89], HTL[90], interface engineering[91] and metal diffusion[92,93]. On the other hand, the observed stability behavior is quite similar to that reported for pin cells not optimized for stability[90,94–96].Thus, all the optimization procedure outlined above can improve the stability also for PSCs with our NiO.

EQE spectra (presented in fig.7) was measured for best performing device made with 10nm NiO. The EQE calculated Jsc is 20.18 mA/cm2, which compare well with the JV measurements at 1 sun (Jsc= 19.68 mA/cm$^2$). We should point out that EQE spectra presents losses in short wavelength 350-450 nm region which is typical for p-i-n MAPbI3 devices caused by parasitic absorption of NiO film[97].

## Experimental

### NiO precursor synthesis

All of the analytical grade were purchased from Sigma-Aldrich and were used as received without further purification.

We used nickel chloride ($NiCl_2$) as a precursor to produce colloid nickel hydroxide ($Ni(OH)_2$) by precipitation in alkaline medium. Freshly prepared nickel hydroxide was rinsed 3 times with deionized water until supernatant became discolored. Then, it was filtered into a paste, which was used without further drying. Nickel acetate ($Ni(CH3COO)_2{\cdot}xH_2O$) was produced by dissolving the paste in 70% acetic acid. The resulting product was purified by recrystallization. Tris(ethylenediamine)nickel complex (TED-NiA) was obtained by direct reaction of 2 g of nickel acetate ($Ni(CH=COOH)_2{\cdot}xH_2O$) with 10 mL of ethylenediamine according to equation 1. The solution changed colour from green to violet, indicating the formation of the complex. Obtained TED-NiA was purified by recrystallization.

$$Ni(CH_3COOH)_2{\cdot}xH2O+3C2H8N2 = [Ni(C_2H_8N_2)_3](CH_3COOH)_2 \quad (1)$$

We analyzed thermal decomposition of obtained nickel complex using thermogravimetric analysis (TGA) to determine water content and decomposition temperature. Fourier transform infrared spectroscopy (FTIR) was used to confirm the transition of nickel acetate to nickel ethylenediamine complex.

### Material, films and device characterization

TGA data was obtained with SDT TA Q600 thermal analyzer. Samples were analyzed in ramp heating mode up to 500 °C, heating rate was set to 10 °C/min. IR spectra was measured on Thermo Nicolet 380 with smart iTR attachment and diamond ATR crystal. All spectra were measured using 32 scans. Spectral range was 650-4000 cm$^{-1}$.

Raman spectra was measured on Thermo DXR Raman Microscope with 523 nm laser. Measurements were done with laser power set to 10 mW.

View Article Online
DOI: 10.1039/C8TC01169A




XRD patterns were collected with tabletop X-Ray spectrometer 'Difray', chromium Kα radiation was used to obtain the data.

SEM images were acquired with JEOL JSM7600F system. Cross section was obtained by using FIB and measured with a FEI Quanta.

Photoluminescence measurements were performed on Cary Eclipse Fluorescence Spectrophotometer with an excitation wavelength of 550 nm.

NiO film thickness was measured on micro interferometer system LOMO MII-4 on polished Si substrates with a metal film on the top.

Auger investigation was performed by Auger nanoprobe PHI-680 "Physical Electronics". The energy of the primary electron beam was $E_0$ = 10 keV with a current density current of 10 nA. For sputtering, we used an argon ion gun with an energy of the primary beam 2 keV, current - 1.4 μA, rastering 1x1 mm ($v_{sput}$ = 20 nm/min for $SiO_2$).

JV curves were measured under standard conditions 1.5 AM G spectra, 100 mW/cm$^2$ of irradiance intensity with Newport ABB solar simulator (calibrated with certified Si cell and Ophir irradiance meter). Scan sweeps were performed with Keithley 2400 SMU and Labview software. A voltage step of 23.5 mV was used for each sweep with a settling time of $10^{-2}$ s.

External quantum efficiency spectra was measured with QEX10 system from PV measurements (calibration by Si certified cell).

**Perovskite ink preparation**

Perovskite ink was prepared in 1.5 M concentration in anhydrous dimethylformamide (DMF from Sigma Aldrich) with $CH_3NH_3I$ (MAI, 99.99 % purity from GreatCellSolar) and PbI2 (ultrapure 99.999 % from TCI). The precursor was heated during 1 hour at 70 °C and then cooled to room temperature prior use.

**Solar cell fabrication**

Solar cells were fabricated in planar inverted architecture on pixelated FTO glass substrates (TEC-8 from Kintec). Firstly, substrates were sonicated in acetone, toluene and isopropyl alcohol and then and activated under UV –ozone treatment during 20 minutes. NiO HTL was decomposed from spin coated TED-NiA. The procedure was the same for all the 3 concentrations (1.0 M; 1.5 M; 2.0 M). The precursor was deposited at 4000 RPM during 1 minute and then annealed at 300 °C during 1 hour.
Perovskite photoactive layer was spin coated from previously described ink in the glove box with solvent engineering method. The perovskite precursor was spin coated at 5000 RPMs during 30 seconds on the glass/FTO/NiO substrate. A 300 μl of anhydrous toluene was dropped on each substrate 8 second after the start of the spin coating to induce the crystallization process. Then samples were annealed at 100°C for 10 minutes. 40nm of C60 ETL was thermally evaporated in a vacuum chamber at 2*10-6 Torr vacuum level. Bathocuproine hole blocking layer and Al were sequentially deposited at same conditions through the mask to form 0.15 cm$^2$ cell pixels. The final thicknesses of the layers were 40 nm for C60, 7.5 nm for BCP and 80 nm for Al.

## Conclusions

In this paper, we study the TED-NiA complex as a new and easy to synthesize precursor for the deposition of NiO thin layer used as HTM in inverted (p-i-n) PSC. TED-NiA provides a perspective strategy for low temperature (280-300 °C) processing of NiO HTL. A thorough material characterization was performed on the NiO precursor and on the NiO film, including TGA, FTIR, Raman, Auger spectroscopy, XRD, SEM and PL. Despite to presence of Carbon and metallic Nickel impurities in NiO layer, a PCE > 15 % was achieved by proper optimization of the NiO thickness down to 10nm. Two effects contribute to the increasing of PCE by reducing the NiO thickness: i) the increase of the FF (up to 0.77) due to the reduction of series resistance from 9.94 Ohm*cm$^2$ for 27nm NiO to 4.61 Ohm*cm$^2$ for 10 nm NiO and ii) the increase of the Jsc due to the improved charge transfer at the Perovskite/NiO interface. Future progresses of this precursor route will be obtained by improving the quality of perovskite layer by the multication approach and finer control over the film chemical composition to drop the annealing temperatures below 250 °C that will make this approach compatible with many flexible substrates.

## Conflicts of interest

There are no conflicts to declare.

## Acknowledgements

The authors gratefully acknowledge the financial support of the Ministry of Education and Science of the Russian Federation in the framework of Megagrant №14.Y26.31.0027.

## Notes and references

1 A. Kojima, K. Teshima, Y. Shirai and T. Miyasaka, *J. Am. Chem. Soc.*, 2009, **131**, 6050–6051.
2 efficiency-chart.png (2219×1229), https://www.nrel.gov/pv/assets/images/efficiency-chart.png, (accessed December 18, 2017).
3 M. Taguchi, A. Yano, S. Tohoda, K. Matsuyama, Y. Nakamura, T. Nishiwaki, K. Fujita and E. Maruyama, *IEEE J. Photovoltaics*, 2014, **4**, 96–99.
4 J. Ramanujam and U. P. Singh, *Energy Environ. Sci.*, 2017,

DOI: 10.1039/C8TC01169A



**10**, 1306–1319.

5 A. Le Donne, A. Scaccabarozzi, S. Tombolato, S. Marchionna, P. Garattini, B. Vodopivec, M. Acciarri and S. Binetti, *ISRN Renew. Energy*, 2013, **2013**, 1–8.

6 N. G. Park, M. Grätzel and T. Miyasaka, *Organic-inorganic halide perovskite photovoltaics: From fundamentals to device architectures*, 2016.

7 T. Leijtens, G. E. Eperon, S. Pathak, A. Abate, M. M. Lee and H. J. Snaith, *Nat. Commun.*, , DOI:10.1038/ncomms3885.

8 S. Kumar and A. Dhar, *ACS Appl. Mater. Interfaces*, 2016, **8**, 18309–18320.

9 T. A. Berhe, W.-N. Su, C.-H. Chen, C.-J. Pan, J.-H. Cheng, H.-M. Chen, M.-C. Tsai, L.-Y. Chen, A. A. Dubale and B.-J. Hwang, *Energy Environ. Sci.*, 2016, **9**, 323–356.

10 A. Baumann, S. Väth, P. Rieder, M. C. Heiber, K. Tvingstedt and V. Dyakonov, *J. Phys. Chem. Lett.*, 2015, **6**, 2350–2354.

11 H. Oga, A. Saeki, Y. Ogomi, S. Hayase and S. Seki, *J. Am. Chem. Soc.*, 2014, **136**, 13818–13825.

12 B. Roose, K. C. Gödel, S. Pathak, A. Sadhanala, J. P. C. Baena, B. D. Wilts, H. J. Snaith, U. Wiesner, M. Grätzel, U. Steiner and A. Abate, *Adv. Energy Mater.*, , DOI:10.1002/aenm.201501868.

13 G. Abdelmageed, L. Jewell, K. Hellier, L. Seymour, B. Luo, F. Bridges, J. Z. Zhang and S. Carter, *Cit. Appl. Phys. Lett. J. Appl. Phys. J. Appl. Phys. J. Appl. Phys*, 2016, **109**, 233905–185901.

14 C. H. Teh, R. Daik, E. L. Lim, C. C. Yap, M. A. Ibrahim, N. A. Ludin, K. Sopian and M. A. Mat Teridi, *J. Mater. Chem. A*, 2016, **4**, 15788–15822.

15 M. Namatame, M. Yabusaki, T. Watanabe, Y. Ogomi, S. Hayase and K. Marumoto, *Appl. Phys. Lett.*, , DOI:10.1063/1.4977789.

16 N. ONOZAWA-KOMATSUZAKI, T. FUNAKI, T. N. MURAKAMI, S. KAZAOUI, M. CHIKAMATSU and K. SAYAMA, *Electrochemistry*, 2017, **85**, 226–230.

17 M. C. Jung and Y. Qi, *Org. Electron. physics, Mater. Appl.*, 2016, **31**, 71–76.

18 S. Cacovich, G. Divitini, C. Ireland, F. Matteocci, A. Di Carlo and C. Ducati, *ChemSusChem*, 2016, **9**, 2673–2678.

19 Z. Li, C. Xiao, Y. Yang, S. P. Harvey, D. H. Kim, J. A. Christians, M. Yang, P. Schulz, S. U. Nanayakkara, C.-S. Jiang, J. M. Luther, J. J. Berry, M. C. Beard, M. M. Al-Jassim and K. Zhu, *Energy Environ. Sci.*, 2017, **10**, 1234–1242.

20 R. T. Ginting, M.-K. Jeon, K.-J. Lee, W.-Y. Jin, T.-W. Kim and J.-W. Kang, , DOI:10.1039/c6ta09202k.

21 L. Meng, J. You, T. F. Guo and Y. Yang, *Acc. Chem. Res.*, 2016, **49**, 155–165.

22 D. Huang, T. Goh, J. Kong, Y. Zheng, S. Zhao, Z. Xu and A. D. Taylor, *Nanoscale*, 2017, **9**, 4236–4243.

23 M. He, B. Li, X. Cui, B. Jiang, Y. He, Y. Chen, D. O'Neil, P. Szymanski, M. A. EI-Sayed, J. Huang and Z. Lin, *Nat. Commun.*, 2017, **8**, 16045.

24 A. S. Subbiah, A. Halder, S. Ghosh, N. Mahuli, G. Hodes and S. K. Sarkar, *J. Phys. Chem. Lett.*, 2014, **5**, 1748–1753.

25 J. H. Heo, H. J. Han, D. Kim, T. K. Ahn and S. H. Im, *Energy Environ. Sci.*, 2015, **8**, 1602–1608.

26 W. Yan, S. Ye, Y. Li, W. Sun, H. Rao, Z. Liu, Z. Bian and C. Huang, *Adv. Energy Mater.*, 2016, 6.

27 N. Arora, M. I. Dar, A. Hinderhofer, N. Pellet, F. Schreiber, S. M. Zakeeruddin and M. Grätzel, *Science (80-. ).*, 2017, **358**, 768–771.

28 S. Ye, W. Sun, Y. Li, W. Yan, H. Peng, Z. Bian, Z. Liu and C. Huang, *Nano Lett.*, 2015, **15**, 3723–3728.

29 P. Wang, J. Zhang, Z. Zeng, R. Chen, X. Huang, L. Wang, J. Xu, Z. Hu and Y. Zhu, *J. Mater. Chem. C*, 2016, **4**, 9003–9008.

30 H. Sun, X. Hou, Q. Wei, H. Liu, K. Yang, W. Wang, Q. An and Y. Rong, *Chem. Commun.*, 2016, **52**, 8099–8102.

31 M. I. Hossain, F. H. Alharbi and N. Tabet, *Sol. Energy*, 2015, **120**, 370–380.

32 I. Y. Y. Bu, Y.-S. Fu, J.-F. Li and T.-F. Guo, *RSC Adv.*, 2017, **7**, 46651–46656.

33 Z.-L. Tseng, L.-C. Chen, C.-H. Chiang, S.-H. Chang, C.-C. Chen and C.-G. Wu, *Sol. Energy*, 2016, **139**, 484–488.

34 J. H. Kim, P. W. Liang, S. T. Williams, N. Cho, C. C. Chueh, M. S. Glaz, D. S. Ginger and A. K. Y. Jen, *Adv. Mater.*, 2015, **27**, 695–701.

35 Y.-H. Chiang, C.-K. Shih, A.-S. Sie, M.-H. Li, C.-C. Peng, P.-S. Shen, Y.-P. Wang, T.-F. Guo and P. Chen, *J. Mater. Chem. A*, 2017, **5**, 25485–25493.

36 J. H. Heo, S.-C. Lee, S.-K. Jung, O.-P. Kwon and S. H. Im, *J. Mater. Chem. A*, 2017, **5**, 20615–20622.

37 Y. Rong, Y. Hu, S. Ravishankar, H. Liu, X. Hou, Y. Sheng, A. Mei, Q. Wang, D. Li, M. Xu, J. Bisquert and H. Han, *Energy Environ. Sci.*, , DOI:10.1039/C7EE02048A.

38 A. Corani, M.-H. Li, P.-S. Shen, P. Chen, T.-F. Guo, A. El Nahhas, K. Zheng, A. Yartsev, V. Sundström and C. S. Ponseca, *J. Phys. Chem. Lett.*, 2016, **7**, 1096–1101.

39 M. YANAGIDA, L. SHIMOMOTO, Y. SHIRAI and K. MIYANO, *Electrochemistry*, 2017, **85**, 231–235.

40 K. Yao, F. Li, Q. He, X. Wang, Y. Jiang, H. Huang and A. K. Y. Jen, *Nano Energy*, 2017, **40**, 155–162.

41 M.-A. Park, I. J. Park, S. Park, J. Kim, W. Jo, H. J. Son and J. Y. Kim, *Curr. Appl. Phys.*, , DOI:10.1016/j.cap.2017.11.010.

42 W. Chen, F. Z. Liu, X. Y. Feng, A. B. Djurišić, W. K. Chan and Z. B. He, *Adv. Energy Mater.*, , DOI:10.1002/aenm.201700722.

43 N. T. Madhu, P. K. Radhakrishnan and W. Linert, in *Journal of Thermal Analysis and Calorimetry*, 2006, vol. 84, pp. 607–611.

44 N. N. Nichio, M. L. Casella, E. N. Ponzi and O. A. Ferretti, *Thermochim. Acta*, 2003, **400**, 101–107.

45 N. S. Gajbhiye and S. Prasad, *Thermochim. Acta*, 1996, **285**, 325–336.

46 A. Fopah Lele, F. Kuznik, H. U. Rammelberg, T. Schmidt and W. K. L. Ruck, *Appl. Energy*, 2015, **154**, 447–458.

47 J. C. De Jesus, I. González, A. Quevedo and T. Puerta, in *Journal of Molecular Catalysis A: Chemical*, 2005, vol. 228, pp. 283–291.

48 W. J. Barreto, H. De Santana, F. A. S. Almeida, D. N. Ishikawa and Y. Kawano, *J. Anal. Appl. Pyrolysis*, 2003, **70**, 199–210.

49 S. A. Sallam, *Transit. Met. Chem.*, 2005, **30**, 341–351.

50 I. T. Ahmed, *J. Anal. Appl. Pyrolysis*, 2007, **80**, 383–388.

View Article Online
DOI: 10.1039/C8TC01169A





51 X. Li, Y. Wu, D. Gu and F. Gan, *Thermochim. Acta*, 2009, **493**, 85–89.
52 S. M. A. Katib, *J. Therm. Anal. Calorim.*, 2011, **103**, 647–652.
53 M. Marciuš, M. Ristić, M. Ivanda and S. Musić, *J. Mol. Struct.*, 2013, **1044**, 231–238.
54 A. D. Khalaji, M. Nikookar and D. Das, *Res. Chem. Intermed.*, 2015, **41**, 357–363.
55 A. Yabuki, Y. Ichida, S. Kang and I. W. Fathona, *Thin Solid Films*, 2017, **642**, 169–173.
56 S. Farhadi and Z. Roostaei-Zaniyani, *Polyhedron*, 2011, **30**, 971–975.
57 V. Zardetto, T. M. Brown, A. Reale and A. Di Carlo, *J. Polym. Sci. Part B Polym. Phys.*, 2011, **49**, 638–648.
58 P. Wu, X. Ma, J. Ji and Y. Ma, *Energy Procedia*, 2017, **105**, 68–74.
59 B. R. Reed, S. A. Stoian, R. L. Lord and S. Groysman, *Chem. Commun.*, 2015, **51**, 6496–6499.
60 N. Dharmaraj, P. Prabu, S. Nagarajan, C. H. Kim, J. H. Park and H. Y. Kim, *Mater. Sci. Eng. B Solid-State Mater. Adv. Technol.*, 2006, **128**, 111–114.
61 J. You, L. Meng, T.-B. Song, T.-F. Guo, Y. (Michael) Yang, W.-H. Chang, Z. Hong, H. Chen, H. Zhou, Q. Chen, Y. Liu, N. De Marco and Y. Yang, *Nat. Nanotechnol.*, 2015, **11**, 75–81.
62 B. G. H. M. Groeneveld, M. Najafi, B. Steensma, S. Adjokatse, H.-H. Fang, F. Jahani, L. Qiu, G. H. ten Brink, J. C. Hummelen and M. A. Loi, *APL Mater.*, 2017, **5**, 076103.
63 X. Yin, Z. Yao, Q. Luo, X. Dai, Y. Zhou, Y. Zhang, Y. Zhou, S. Luo, J. Li, N. Wang and H. Lin, *ACS Appl. Mater. Interfaces*, 2016, acsami.6b13372.
64 Q. Wang, C.-C. Chueh, T. Zhao, J. Cheng, M. Eslamian, W. C. H. Choy and A. K.-Y. Jen, *ChemSusChem*, 2017, **10**, 3794–3803.
65 S. Seo, I. J. Park, M. Kim, S. Lee, C. Bae, H. S. Jung, N.-G. Park, J. Y. Kim and H. Shin, *Nanoscale*, 2016, **8**, 11403–11412.
66 F. Nazli DInçer Kaya, I. Svoboda, O. Atakol, Ü. Ergun, A. Kenar, M. Sari and K. C. Emregül, *J. Therm. Anal. Calorim.*, 2008, **92**, 617–624.
67 J. Zhang, H. Luo, W. Xie, X. Lin, X. Hou, J. Zhou, S. Huang, W. Ou-Yang, Z. Sun and X. Chen, *Nanoscale*, , DOI:10.1039/C7NR08750K.
68 Y. Bai, H. Chen, S. Xiao, Q. Xue, T. Zhang, Z. Zhu, Q. Li, C. Hu, Y. Yang, Z. Hu, F. Huang, K. S. Wong, H. L. Yip and S. Yang, *Adv. Funct. Mater.*, 2016, **26**, 2950–2958.
69 W. Nie, H. Tsai, J. C. Blancon, F. Liu, C. C. Stoumpos, B. Traore, M. Kepenekian, O. Durand, C. Katan, S. Tretiak, J. Crochet, P. M. Ajayan, M. Kanatzidis, J. Even and A. D. Mohite, *Adv. Mater.*, , DOI:10.1002/adma.201703879.
70 W. R. Pease, R. L. Segall, R. S. C. Smart and P. S. Turner, *J. Chem. Soc. Faraday Trans. 1 Phys. Chem. Condens. Phases*, 1986, **82**, 747.
71 Z. J. Huba and E. E. Carpenter, *Dalt. Trans.*, 2014, **43**, 12236–12242.
72 M. M. Lacerda, F. Kargar, E. Aytan, R. Samnakay, B. Debnath, J. X. Li, A. Khitun, R. K. Lake, J. Shi and A. A. Balandin, *Appl. Phys. Lett.*, 2017, **110**, 202406.
73 J. Tientong, S. Garcia, C. R. Thurber and T. D. Golden, *J. Nanotechnol.*, 2014, **2014**, 1–6.
74 J. T. Richardson, R. Scates and M. V Twigg, *Appl. Catal. A Gen.*, 2003, **246**, 137–150.
75 Q.-D. Yang‡, J. Li, Y. Cheng, H.-W. Li, Z. Guan, B. Yu and S.-W. Tsang, *J. Mater. Chem. A*, 2017, **5**, 9852–9858.
76 J. Zhang and T. Pauporté, *J. Phys. Chem. C*, 2015, **119**, 14919–14928.
77 E. Thimsen, A. B. F. Martinson, J. W. Elam and M. J. Pellin, *J. Phys. Chem. C*, 2012, **116**, 16830–16840.
78 M. Jlassi, I. Sta, M. Hajji and H. Ezzaouia, *Mater. Sci. Semicond. Process.*, 2014, **21**, 7–13.
79 K. C. Icli and M. Ozenbas, *Electrochim. Acta*, , DOI:10.1016/j.electacta.2018.01.073.
80 H.-S. Kim, J.-Y. Seo, H. Xie, M. Lira-Cantu, S. M. Zakeeruddin, M. Grätzel and A. Hagfeldt, *ACS Omega*, 2017, **2**, 9074–9079.
81 Y. Shao, Z. Xiao, C. Bi, Y. Yuan and J. Huang, *Nat. Commun.*, 2014, **5**, 1–7.
82 F. Meng, K. Liu, S. Dai, J. Shi, H. Zhang, X. Xu, D. Li and X. Zhan, *Mater. Chem. Front.*, 2017, **1**, 1079–1086.
83 K. Lee, J. Ryu, H. Yu, J. Yun, J. Lee and J. Jang, *Nanoscale*, 2017, **9**, 16249–16255.
84 M. Pelton and G. W. Bryant, *Introduction to metal-nanoparticle plasmonics*, .
85 X. Xiang, X. T. Zu, S. Zhu, C. F. Zhang and L. M. Wang, *Nucl. Instruments Methods Phys. Res. Sect. B Beam Interact. with Mater. Atoms*, 2006, **250**, 229–232.
86 Z. Xiong, X. Chen, X. Wang, L. Peng, D. Yan, H. Lei, Y. Fu, J. Wu, Z. Li, X. An and W. Wu, *Appl. Surf. Sci.*, 2013, **268**, 524–528.
87 Y. Liu, F. Lang, T. Dittrich, A. Steigert, C.-H. Fischer, T. Köhler, P. Plate, J. Rappich, M. C. Lux-Steiner and M. Schmid, *RSC Adv.*, 2017, **7**, 1206–1214.
88 M. Saliba, T. Matsui, J.-Y. Seo, K. Domanski, J.-P. Correa-Baena, M. K. Nazeeruddin, S. M. Zakeeruddin, W. Tress, A. Abate, A. Hagfeldt and M. Grätzel, *Energy Environ. Sci.*, 2016, **9**, 1989–1997.
89 M. Alsari, A. J. Pearson, J. T.-W. Wang, Z. Wang, A. Montisci, N. C. Greenham, H. J. Snaith, S. Lilliu and R. H. Friend, *Sci. Rep.*, 2018, **8**, 5977.
90 S. Peng, J. Miao, I. Murtaza, L. Zhao, Z. Hu, M. Liu, T. Yang, Y. Liang, H. Meng and W. Huang, *J. Mater. Chem. C*, 2017, **5**, 5949–5955.
91 G. Kakavelakis, I. Paradisanos, B. Paci, A. Generosi, M. Papachatzakis, T. Maksudov, L. Najafi, A. E. Del Rio Castillo, G. Kioseoglou, E. Stratakis, F. Bonaccorso and E. Kymakis, *Adv. Energy Mater.*, 2018, 1702287.
92 E. Bi, H. Chen, F. Xie, Y. Wu, W. Chen, Y. Su, A. Islam, M. Grätzel, X. Yang and L. Han, *Nat. Commun.*, 2017, **8**, 15330.
93 W. Ming, D. Yang, T. Li, L. Zhang and M.-H. Du, *Adv. Sci. (Weinheim, Baden-Wurttemberg, Ger.*, 2018, **5**, 1700662.
94 G. Niu, S. Wang, J. Li, W. Li and L. Wang, *J. Mater. Chem. A*, 2018, **6**, 4721–4728.
95 F. Matsumoto, S. M. Vorpahl, J. Q. Banks, E. Sengupta and D. S. Ginger, *J. Phys. Chem. C*, 2015, **119**, 20810–20816.
96 Z. Zhu, C.-C. Chueh, F. Lin and A. K.-Y. Jen, *Adv. Sci.*, 2016,

DOI: 10.1039/C8TC01169A


**3**, 1600027.

97 X. Yin, Z. Yao, Q. Luo, X. Dai, Y. Zhou, Y. Zhang, Y. Zhou, S. Luo, J. Li, N. Wang and H. Lin, *ACS Appl. Mater. Interfaces*, 2017, **9**, 2439–2448.

View Article Online
DOI: 10.1039/C8TC01169A




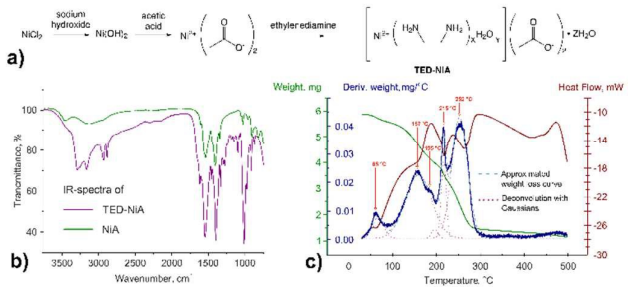


Fig.1. (a) Synthesis route of TED-NiA precursor for HTL fabrication, (b) FTIR spectra of Nickel acetate and synthesed TED-NiA, (c) Thermogravimetric analysis results for TED-NiA decomposition in dry air atmosphere with derivative weight and heat flow curves

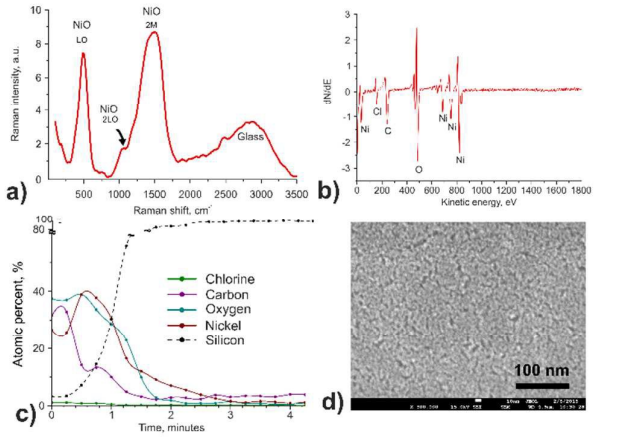


**Fig. 2.** (a) Raman spectra of NiO film decomposed from TED-NiA precursor on glass, (b) Auger spectrum of NiO compact layer on Si wafer, (c) Compositional depth profile obtained with Auger spectroscopy of the NiO film on Si wafer, (d) SEM image of NiO film

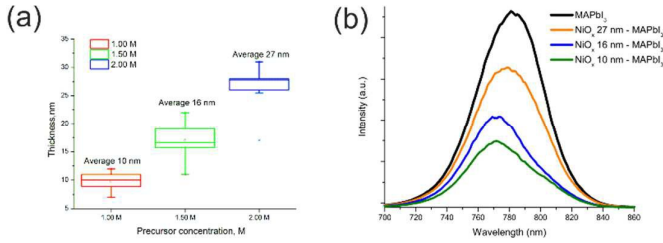


Fig.3. (a) NiO film thickness as a function of TED-NiA precursor concentration, (b) Photoluminescence spectrum of perovskite $MAPbI_3$ film on NiO/FTO/glass stack for different thickness of NiO. The black curve refer to the $MAPbI_3$/FTO/glass stack

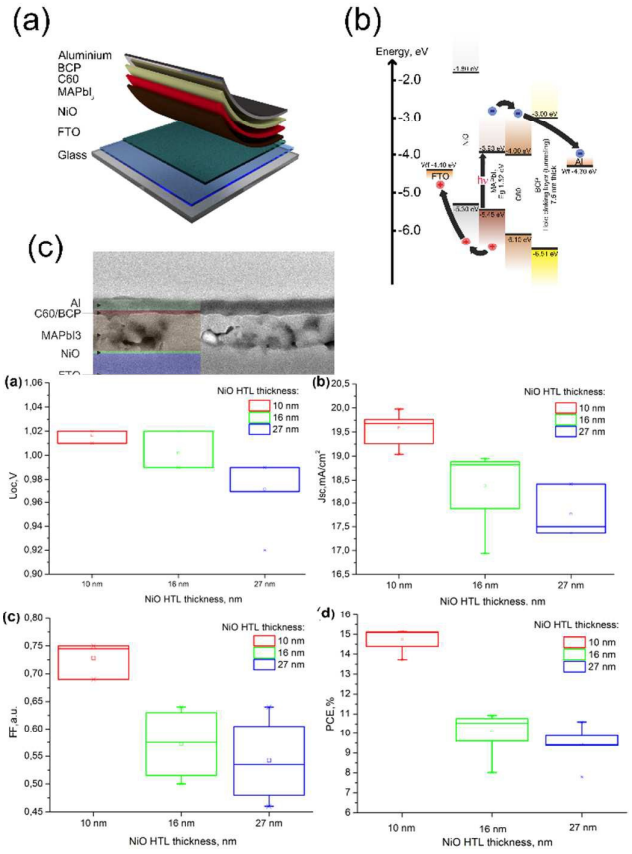


Fig.5. Box-plot of photovoltaic parameters of the fabricated devices for several NiO HTL thicknesses, (a) Voc, (b) for Jsc, (c) for FF, (d) for PCE

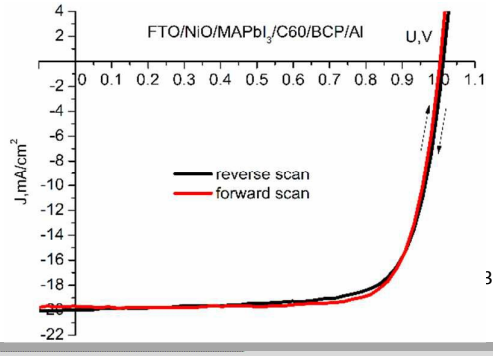


Fig. 6. JV curve of best performing PSC with 10 nm thick NiO HTL

View Article Online
DOI: 10.1039/C8TC01169A



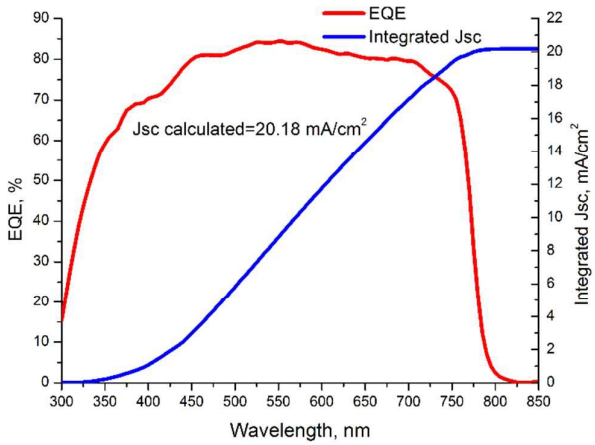


Fig. 7. EQE spectra and integrated Jsc plot of best performing PSC with 10 nm thick NiO HTL

View Article Online
DOI: 10.1039/C8TC01169A



**Entry for the Table of Contents**

**Tris (ethylene diamine) nickel acetate as a promising precursor for hole transport layer in planar structured perovskite solar cells**

## Novelty:

NiO/Perovskite interface was investigated with Auger profiling for pin solar cell with PCE >15% and fabricated with novel HTL precursor.

Layout 1:

FULL PAPER



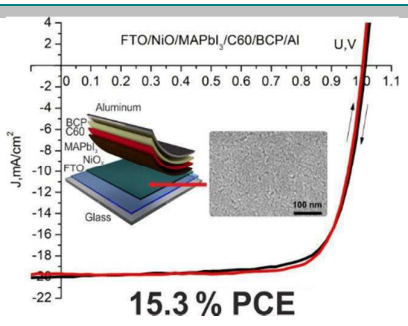


Danila S. Saranin*[a], Vsevolod N. Mazov[a], Lev O. Luchnikov[a], Sergei Lypenko[b], Pavel A. Gostishev[a], Dmitry S.Muratov[a], Dmitry A. Podgorny[c], Denis M. Migunov[d], Sergei I. Didenko[a][e], Marina N. Orlova[e], Denis V. Kuznetsov[a][f], Alexey R. Tameev[b] and Aldo Di Carlo*[a],[g]

***Page 1. – Page 9.***

**Title: Tris (ethylene diamine) nickel acetate as a promising precursor for hole transport layer in planar structured perovskite solar cells**